Materials Chemistry and Physics 205 (2018) 72–83

Contents lists available at ScienceDirect

Materials Chemistry and Physics

journal homepage: www.elsevier.com/locate/matchemphys

Dielectric relaxation study of the ceramic matrix $BaBi_4Ti_4O_{15}$:Bi_2O_3

P.M.V. Almeida [a], C.B. Gozzo [b], E.H.N.S. Thaines [b], A.J.M. Sales [c], R.G. Freitas [b], A.J. Terezo [b], A.S.B. Sombra [d], M.M. Costa [b, e, *]

[a] Federal University of Rondônia, Department of Physics of Ji-Paraná - RO, 78960-000, Brazil
[b] Federal University of Mato Grosso - UFMT, Department of Chemistry, Cuiaba, MT, Brazil
[c] I3N and Physics Department, Aveiro University, Campus Universitário de Santiago, Aveiro, Portugal
[d] Tele Informatics Engineering Department (DETI), Federal University of Ceará, UFC, 60455-760 Fortaleza, CE, Brazil
[e] Institute of Physics, LACANM, UFMT, 78060-900 Cuiabá, MT, Brazil

HIGHLIGHTS

- Dielectric properties of a $BaBi_4Ti_4O_{15}$ ceramic were investigated.
- Effect of excess bismuth oxide (1−10 wt%) in the ceramics.
- Rietveld refinement observed increase in the parameter c/a.
- Structural phase transition observed at 450 °C.
- DC conductivity with temperature confirms the Arrhenius behavior.

GRAPHICAL ABSTRACT

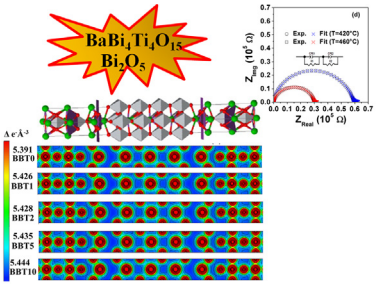

ARTICLE INFO

Article history:
Received 14 June 2017
Received in revised form
10 October 2017
Accepted 29 October 2017
Available online 7 November 2017

Keywords:
Impedance spectroscopy
X-ray methods
Dielectric relaxation
Electrical conductivity

ABSTRACT

The dielectric properties of a $BaBi_4Ti_4O_{15}$ ceramic were investigated at data temperature range from 340 to 520 °C. The effect of excess bismuth oxide (1−10 wt%) in the ceramics by solid state reaction has been investigated. Rietveld refinement observed increase in the fundamental crystallographic parameter c/a of the 10.8074 up to 10.8900 for BBT, compared to BBT-doped materials. The complex studies of impedance exhibit electrical properties of the material are strongly dependent on temperature. The temperature dependence of the dielectric permittivity showed the presence of a structural phase transition that was observed at near 450 °C. The decrease in value of grain and grain boundary resistance with increasing temperature suggests the existence of an increase of the conductivity. The nature of variation of DC conductivity with temperature confirms the Arrhenius behavior of the material. The DC electrical and thermal conductivity of grain and grain boundary have been assessed.

1. Introduction

The bismuth layer-structured ferroelectrics, described as $(Bi_2O_2)^{2+}(A_{m-1}B_mO_{3m+1})^{2-}$, is often used in application for ferroelectric random access memories (FeRAMs) and high-temperature piezoelectric devices. This is due to their fast switching speed, significant remaining polarization, low operating voltage, low coercive field, high Curie temperature and superior polarization fatigue resistant characteristics [1-3,26,37].

Bismuth-layered crystal structures (and their properties) have been investigated in detail in the literature as ferro electrics with a high Curie temperature. The formation of a short bond between the

* Corresponding author. Federal University of Mato Grosso - UFMT, Department of Chemistry, Cuiaba, MT, Brazil.
E-mail address: mauro48@gmail.com (M.M. Costa).

https://doi.org/10.1016/j.matchemphys.2017.10.069
0254-0584/

apex oxygen in the perovskite layer and the bismuth in the $[Bi_2O_2]^{2+}$ layers, can be explained with octahedral rotations and A-site cationic displacements [4,5].

These oxides are described in general terms as a pseudo-perovskite block, $(A_{m-1}B_mO_3m_{+1})^{2-}$ sandwiched between bismuth oxide layers $(Bi_2O_2)^{2+}$oriented along the *c*-axis, where the value of *A* is mono-, di-, or trivalent large cation with 12-fold coordination, *B* is tetra-, penta-, or hexavalent small cation with octahedral coordination and *m* may vary between 2 and 5 that corresponds to the number of BO_6 octahedral layers in the perovskite blocks.

Aurivillius oxides are described in the literature as exhibit relaxor behavior such as $BaBi_2Ta_2O_9$, $BaBi_2Nb_2O_9$, $BaBi_4Ti_4O_{15}$ etc. [6–8]. Relaxor ferroelectrics are materials that in recent years have been attracting the attention of researchers for a wide range of applications. Considering its properties in excellent piezoelectric responses and high dielectric over a wide range of temperature. Relaxor ferroelectrics have a broad dielectric permittivity maximum temperature (*Tm*) with a frequency dispersion on the lower side of *Tm*.

The phenomenon in ferroelectric materials exists when there occurs a delay in the frequency response of a group of dipoles when submitted to an externally applied field. When an alternating voltage is submitted to a dielectric, the dipoles responsible for the polarization do not follow the oscillations of the electric field at the same frequencies. In this way, the field reversal and the dipole reorientation becomes out-of-phase; this fact causes a dissipation of energy.

In ferroelectric materials, the dielectric relaxation mechanisms contribute significantly to factors such as: i) ionic substitution; ii) structural defects; iii) electric field and iv) temperature. These defects can occur on either intrinsic or extrinsic heterogeneities due to preparation in material rates, as rates of heating and treatments that can influence ionic substitutions, grain and grain boundary nature. However, structural defects can modify short and/or long-range interactions in materials with ferroelectrics properties.

In reviewing the research, many studies exist, indicating that a significant amount of work has been completed on the temperature behavior of $BaBi_4Ti_4O_{15}$ (BBT) ceramics. However,few studies exist that discuss the phenomenon of dielectric relaxation and conduction mechanisms.

The use of impedance spectroscopy to describe and analyze dielectric properties of the grain, grain boundary and effects; may be associated with the contribution of electrodes to the response of ceramic materials. To study the intrinsic properties influencing an electrode dielectric system such as: i) dielectric permittivity, ii) conductivity, and iii) the charge carrier's mobility, impedance spectroscopy is very important when interpreting the microscopic processes in order to discern between localized and non-localized conduction processes [9]. To better understand the results, one way is using an equivalent circuit consisting of elements that can be modeled in order to enable one to extract information about the physical properties of the system [10].

There is a significant body of research on the dielectric properties and crystal structure of BBT. However, the published studies only show its diffuse phase transition-relaxor behavior [11–14]. Recently Khokhar et al. [15] reported on the effect excess of bismuth in BBT ceramics and achieved a high dielectric permittivity, low loss factor, and low DC conductivity with 6-8 wt% of excess of bismuth oxide.

Here we present the results of impedance spectroscopy measurements to investigate the influence of bismuth oxide on the electrical properties of barium bismuth titanate ceramics. Analysis of complex impedance and electric modulus using an equivalent circuit model; here, two relaxation processes were identified over the frequency range $1 - 1$ MHz in the electrical properties.

2. Experimental procedures

Polycrystalline ceramics of barium bismuth titanate, $BaBi_4Ti_4O_{15}$, were prepared by the solid-state reaction route with bismuth doping in concentration of x = 1, 2, 5 and 10 wt%. Stoichiometric amounts of reagent grade BaO, Bi_2O_3, and TiO_2 (purity > 99%) were weighed and milled using Pulverisette 5-Fritsch in reactors with spheres of zirconium oxide, being 97.5 g of spheres for each 10 g of material. The grinding was performed at a speed of 360 rpm for 6hs. Following the grinding, the material was dried for one night and calcined at 850 °C in an alumina crucible for 3.0 hs, (heating rate 5 °C/min) and then cooled to room temperature (cooling rate 5 °C/min). The samples were prepared with (0, 1, 2, 5 and 10 wt%) of Bi_2O_3dopant [BBT0, BBT1, BBT2, BBT5 and BBT10] added to the calcined powder then cold pressed into disks of about 1 mm in thickness and 12 mm in diameter at a pressure of about 4 tons for 5 min (346.8 MPa) using polyvinyl alcohol as a binder. The pressed pellets were sintered in air at 950 °C for 3hs (heating rate 5 °C/min until 500 °C and after 3 °C/min) and then cooled to room temperature (cooling rate 5 °C/min). X-ray powder diffraction (Bruker-D8 Advance, with CuK_α radiation $\lambda = 0.154$ nm), was performed using current of 40 KA, voltage of 40 KV, 2θranging from 20 to 80and time step of 0.5 to 0.2, and to find the phase of the calcined power and sintered BBTdoped with Bi_2O_3.

To compare the experimental data with the data from the literature, we used the general structure analysis system (GSAS) program [16] suite with the EXPGUI interface for Rietveld structural refinement [17]. The Rietveld formulation [18], will treat the diffraction line width as a smooth function of the *d*-spacing of the diffraction angle (2θ). Many peaks of interest have presented different widths. Hence, in this work, the peak profile function developed by Stephens et al. [19] was used as a model for investigating the experimental data. With this method, considerations are made for diffraction widths that are not a smooth function of *d*; these effects in X-ray diffraction peaks might arise from anisotropic sample size broadening, or from a particular pattern of defects (e.g. stacking faults). Finally, we used the bi-dimensional model described by Larson & von Dreele [16] to account for the anisotropy in the half width of the reflections.

To investigate the electron density maps we used the model described in literature [20]. The point (*x, y, z*) of the crystallite cell with volume (*V*) is calculated by the Fourier series using the structural factors *F*(*h, k, l*):

$$\rho(x,y,z) = V^{-1}\sum_{k,k,l} F(h,k,l)\exp[2\pi i(hx,ky,lz)] \quad (1)$$

where (*x, y, z*) represents a vector (***r***) of real space, with one vector space (*a*, *b*, *c*) and another vector (***h***, ***k***, ***l***), which represent the coordinates of one vector from the reciprocal space with base (a^*, b^*, c^*), which then coordinates from the diffraction plane given by Bragg's Law. The electron density maps the distribution in the base plane {slice 1 with X = 0 (i.e. face *bc*), with a set (*hkl*) as the projection plane (100)} were calculated by GSAS program [16] from XRD data for BBT0, BBT1, BBT2, BBT5 and BBT10 oxide nanomaterials.

We then applied silver paste on both sides of the circular surfaces of the samples. Forming out the electrical contacts and were cured at 200 °C for 1 h. Temperature dependent dielectric properties were measured up to 500 °C using a Solartron 1260 coupled to a furnace and controlled by computer with a thermostat over 1–1 MHz frequency and a range of temperature 30–500 °C.

The complex impedance Z* and complex electric modulus M* of the sample were obtained by using the relationships:

$$\mathbf{Z}^* = \boldsymbol{Z_{Real}} - \mathbf{j}\boldsymbol{Z_{Imag}} = \frac{1}{\mathbf{j}\omega\mathbf{Co}\varepsilon^*} \quad (2)$$

and

$$M^* = M_{Real} + jM_{Imag} = \frac{1}{\varepsilon^*} = j\omega CoZ^* \quad (3)$$

where Z_{Real} and Z_{Imag} are the real and imaginary parts of the complex impedance ($\boldsymbol{Z}^*$), ω is the angular frequency ($2\pi f$),ε^* is the vacuum permittivity and Co is the vacuum capacitance of the measuring cell. The impedance data analysis was carried out with the ZView 3.1 software package, and the spectra were fitted by means of a complex, non-linear, least-squares procedure.

We study the microstructural characterization in the samples fractured unpolished using a field emission gun scanning electron microscopic (FE-SEM).

3. Results and discussion

3.1. X-ray diffraction

Fig. 1 shows X-ray diffraction (XRD) patterns of polycrystalline $BaBi_4Ti_4O_{15}$ recorded at room temperature (ICSD-24738) and all the compositions. Comparing the results with the experimental data from the literature suggests that the pattern indicated during the analysis shows all the reflections are identified, in good agreement with the tetragonal structure with a space group of 14/mmm. The dominant diffraction peaks of BBT were in good agreement. However, there are studies in the literature that suggest the BBT is a ferroelectric polar material with large polarization. In addition, the synchrotron powder X-ray and neutron powder diffraction (NPD) results on BBT single crystal, also suggest the space group F2mm [21] or A21am [22].

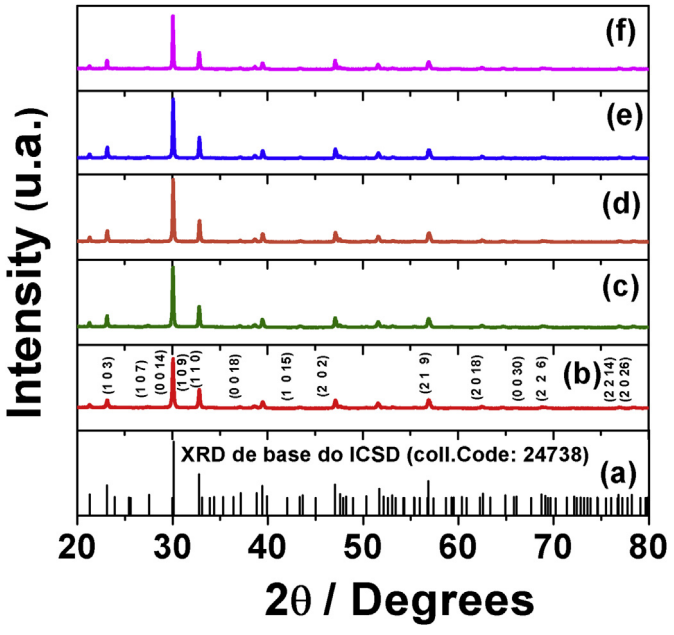

Fig. 1. Room temperature X-ray power diffraction pattern of $BaBi_4Ti_4O_{15}$ ceramics.(a) standard powder diffraction data of the base of the ICSD (Code 24738), (b) BBT0, (c) BBT1, (d) BBT2 (e) BBT5, (f) BBT10.

Fig. 2 shows the behavior of the full width at half maximum (FWHM) for all samples. It can be seen that the full width at half maximum peak [109] for BBTO, BBT1, BBT2, BBT5 and BBT10 sample materials were slightly shifted towards low diffract angle direction. This suggests that by increasing the Bi_2O_3 dopant levels, the expansion of the unit cell is likely related to its incorporation in accordance with similar distortion in perovskite [23]. The results we observed suggest that bismuth ions are basically occupied in the pseudo perovskite layer of $BaBi_4Ti_4O_{15}$ lattice. The peak in (109) plane shows the highest intensity, the increase in peak intensity is a strong indication of the presence of excess bismuth. Similar results were found in the literature to m = 4 [24].

The Fig. 3a shows the Rietveld refinement along with a difference plot taken from the calcined power sample, and the theoretical results. However, the difference between the experimental X-ray profile patterns observed and the theoretically calculated data showed differences close to zero in the of intensity peak, as illustrated by a line ($Y_{observed}-Y_{calculated}$) and statistical parameters (R_{wp} and χ^2). The Rietveld method is a least squares refinement procedure, where the experimental step-scanned values are adapted to the calculated values.

The most important features obtained by the results of refinement also conclude that the present system contains the tetragonal structure. According to the crystallographic information file (CIF 24738-ISCD) obtained for $BaBi_4Ti_4O_{15}$ tetragonal phase (I4/mmm-139), the *a*- and *c*-axes lattice parameters were $a = 3.864$ Å and $c = 41.759$ Å, which lead to a fundamental crystallographic parameter $c/a = 10.807$. However, doping process in perovskites materials leads to an increase in both *a*- and *c*-lattice parameters. In the present study, the crystallographic parameter *c*/*a* obtained were 10.88404 (BBT0), 10.88415 (BBT1), 10.88573 (BBT2), 10.88743 (BBT5) and 10.89006 (BBT10) increasing as a result of the doping content. Such results are in agreement with previous data presented in Fig. 2. Tomkiewicz et al. [25] studied a class of $A_{n+1}B_nO_{3n+1}$, such as $LaSrCo_{0.5}Fe_{1.5}O_{4-\delta}$ ($n = 1$), $La_{0.3}Sr_{2.7}CoFeO_{7-\delta}$ ($n = 2$) and $LaSr_3Co_{1.5}Fe_{1.5}O_{10-\delta}$ ($n = 3$), and observed increasing in the *a*- and *c*-lattice parameters for similar perovskites materials.

Electron density maps of Fourier are important for the determination of precise atomic positions and structural elucidations about the materials. Moreover, a typical pseudo-perovskite block $(A_{m-1}B_mO_{3m+1})^{2-}$, sandwiched between the bismuth oxide layer $(Bi_2O_2)^{2+}$ along the *c*-axis, was observed. Where *m* indicates the

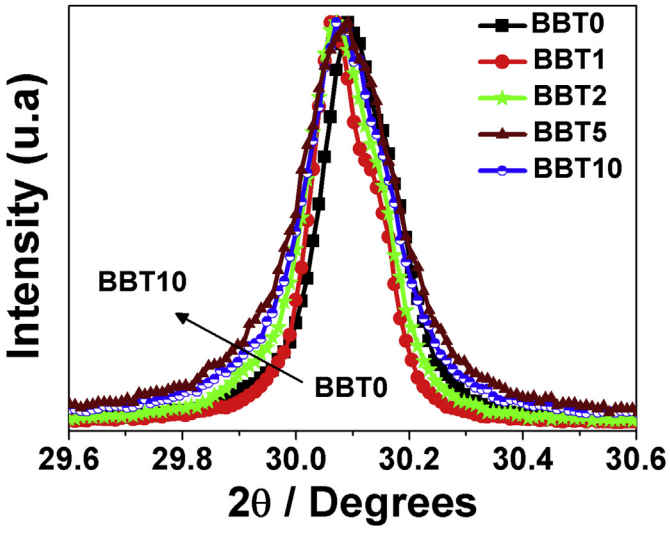

Fig. 2. FWMH peak shifting towards low diffraction angle.

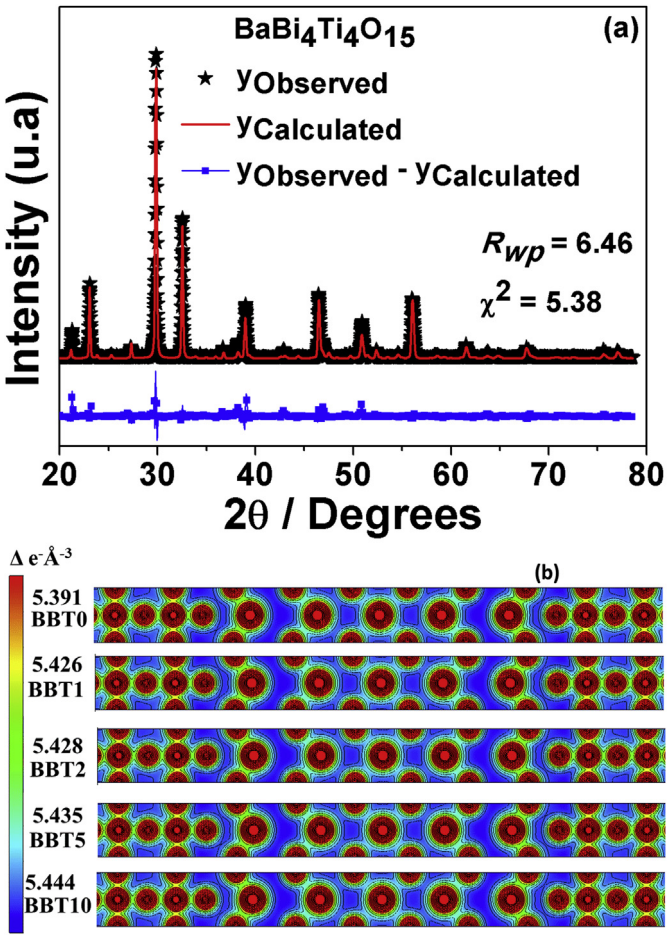

Fig. 3. a) Rietveld refinement plot for BBT and b) electron density maps of Fourier for BBT and dopants content.

number of corner sharing BO_6octahedral forming the perovskite like slabs [5]. On the other hand, Rietveld refinement is also important to notice differences in the electron density for a set of materials such as BBT and doping content. It can be observed in Fig. 3b that although the electron density maps of Fourier look similar, there is an increase in the depth values along *a*-axis for BBT (5.391 $\Delta e^- Å^{-3}$) compared to BBT-doping content such as: BBT1 (5.426 $\Delta e^- Å^{-3}$), BBT2 (5.428 $\Delta e^- Å^{-3}$), BBT5 (5.435 $\Delta e^- Å^{-3}$) and BBT10 (5.444 $\Delta e^- Å^{-3}$). Therefore, the electron density increases as increasing the dopant content. As a result, it can lead to a decrease in the electron transport impedance, higher time constant (related to grain and grain boundary), and higher conductivity; as indeed, we observed in BBT10 compared to BBT. The pronounced effect of dopant levels, and its electrical properties mentioned herein, will be discussed further.

3.2. Impedance

Complex impedance spectroscopy (CIS) is a technique to study the electrical processes and conduction mechanism in materials. This technique is very important because it allows for a separation of the electrical response attributed to the grains (bulk), grain boundary, and electrode polarization on a polycrystalline sample presenting a different relaxation time [9].

This techniques are often employed when analyzing dielectric properties of polycrystalline material and their interfaces with electronically conducting electrodes in a wide range of frequencies (1 –1 MHz),and at different temperatures (340–520 °C). Only the impedance data for BBT0 and BBT10 are indicated here. However, these data are representative for all compositions.

Fig. 4a and b shows the temperature dependence of the real part of impedance (Z_{Real}) with frequency in different temperatures. Comparing both results, it can be clearly seen that the addition of bismuth oxide decreases the value of the impedance. This behavior has been observed for different concentrations of bismuth oxide. A decrease in the value of (Z_{Real}) with increasing temperature and frequency is responsible for an increase in the AC conductivity of the materials. When this happens, it can be related to the existence of negative temperature coefficient of resistance behavior, and all curves merge in the higher-frequency (>10^3 Hz) independent of the change in temperature. The values at higher frequencies for all temperatures observed is associated with a possible release of space charge polarization at high temperatures and frequencies. The behavior of the Z_{Real} indicates the existence of a frequency relaxation process existing in the material. The data shows the existence of more than one relaxation process; this result will be confirmed in the Nyquist plot to be showed in (Fig. 8) along with the discussion. Fig. 5a and b show the temperature dependence of the imaginary impedance (Z_{Imag}) with frequency in different temperatures. The BBT10 sample shows the existence of two relaxation

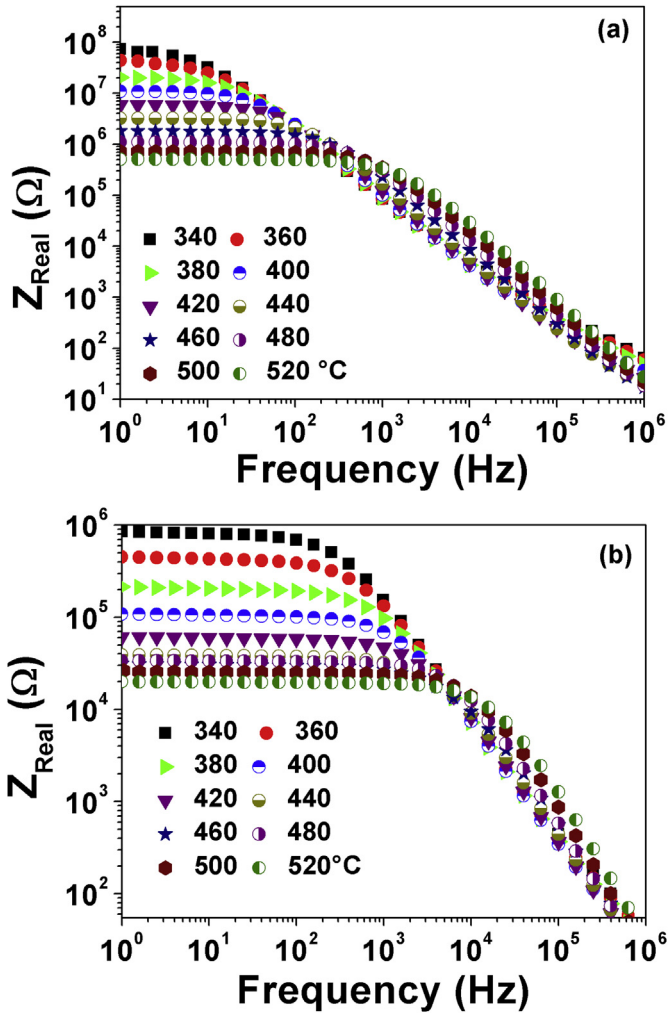

Fig. 4. Variation of Z_{Real} with frequency at different temperatures: (a) for BBT0 and (b) BBT10.

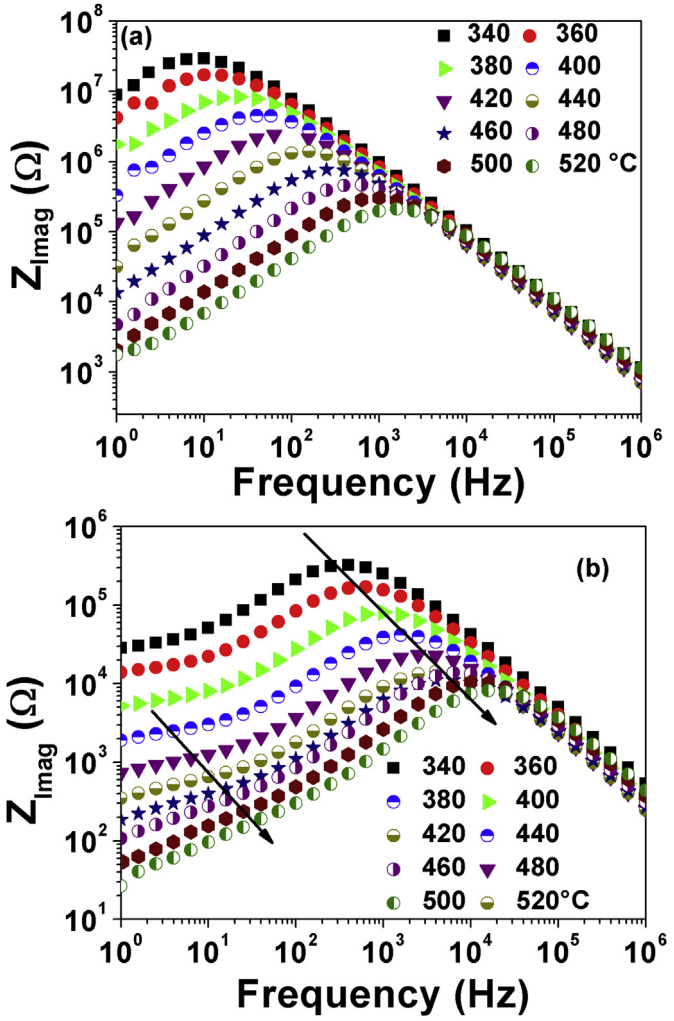

Fig. 5. Variation of Z_{Imag} with frequency at different temperatures: (a) for BBT0 and (b) BBT10.

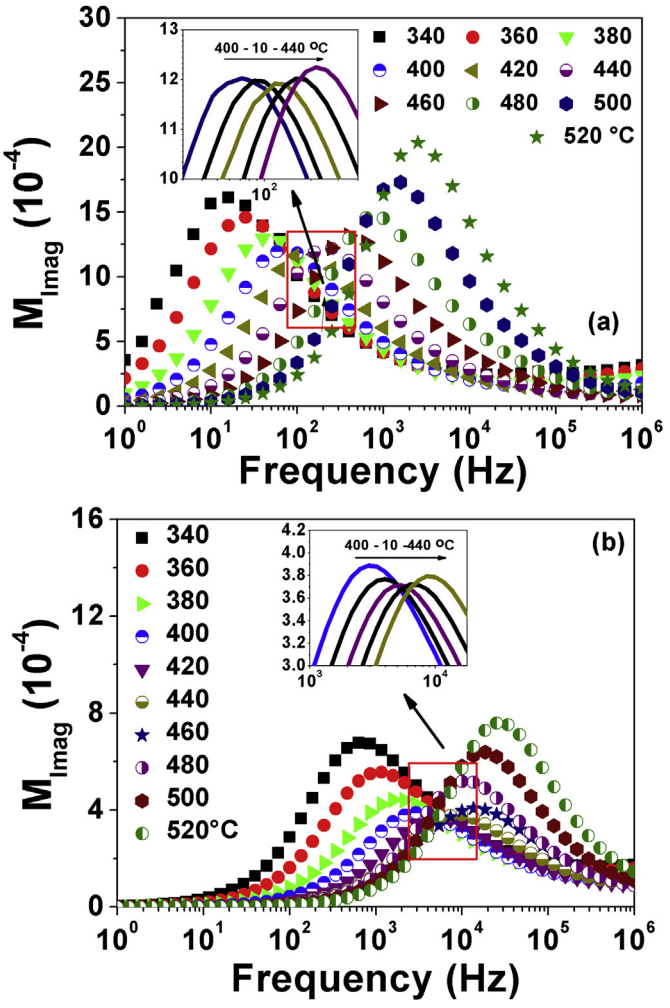

Fig. 6. Variation of M_{Imag} with frequency at different temperatures for: a) BBT0 and b) BBT10.

processes and is more evident. The first (peak) occurs in the low frequency region and another (peak) occurs in the region of highest frequency,as indicated by the arrows. In Fig. 5b the imaginary part of the impedance shows the appearance of two peaks, and that the peaks move to the higher-frequency side with increasing temperature. The maximum value of Z_{Imag} decreases as temperature increases. Her, it is important to notice that the first peak is a typical broad peak, and the second peak an atypical symmetric peak. A decrease in the height of the peaks and the coincidence of all curves above 10 kHz is associated with increasing Bi_2O_3.

The increase in the broadening of the peaks with changes in concentration suggest the presence of a concentration dependent relaxation process in the materials, with 10% of bismuth oxide. The asymmetric broadening of the first peak suggests the presence of electrical processes in the material with spread of relaxation time as indicated by the peak width [26]. The peak at a higher frequency is associated with the grain, while the peak ata lower frequency is associated with the grain boundary. It is important to note that only the grain process is visible in the electric modulus response as shown in Fig. 6.

3.3. Modulus

To investigate the effect of polarization of electrodes and effects that occur on the grain boundary, we have adopted the use the complex electric modulus formalism, it is very important to investigate bulk properties as apparent from conductivity relaxation times [27]. The variation of the real part of the electric modulus (M_{Real}) as a function of frequency over a range of temperatures is not shown here, but it exhibits an expected behavior, M_{Real} approaches zero in the low frequency region and as the frequency increases and this value increase and reaches a maximum constant value of $M_{\infty=1/\varepsilon_\infty}$ higher frequencies regions for all temperatures.

Fig. 6a and b shows the variation of the imaginary part of the electric modulus (M_{Imag}) as a function of frequency over a range of temperature. It is observed that the height of the peak decreases and shifts to higher frequencies until it reaches the temperature Tm (shown in figure). After the temperature *Tm*, the peak value increases and continues shifting to higher frequencies with temperature increase. This result is consistent for all of the samples in this study. The region where the inversion in the magnitude of the peak is linked to a phase transition in the material. The grain (bulk) process is viewed in the electric modulus response as shown in Fig. 6. Since the peak due to the grain is not observed in the imaginary part of the dielectric permittivity, this relaxation is probably associated with the conductive process. In this way, the use of the formalism of the module complex is very important in the analysis of polycrystalline materials.

3.4. Modulus and impedance

Sinclair and West [27] shown that the frequency dependence of the imaginary impedance is useful to detect the effect of the smallest capacitance and the largest resistance. This behavior occurs between a relaxation processes that is related to the short range or long-range movement of charge carriers. When a long-range process occurs, the peak in both plots will occur at the same frequency and if the process is in a short-range scale, these peaks will occur at different frequencies. The best way to show these results is to build a graph of the variation of the imaginary part electric modulus (M_{Imag}) and the imaginary part of impedance (Z_{Imag}) as a function of frequency;this results is shown in the Fig. 7a and b. In the BBT10 composition; the two peaks at different temperatures indicate the presence of short-range motion of charge carries.

The separation between these peaks suggests the presence of localized movement of charge carriers and departure from the ideal Debye-like behavior for all compositions modified with Bi_2O_3. The broad and asymmetric peaks shown in the data irrespective of the Bi_2O_3 concentrations, suggest with results the existence of a distribution of relaxation times. In Fig. 5, it was observed that the appearance of more than one defined peak occurred at lower temperatures with increasing Bi_2O_3. The data presented in descending order of temperature on increasing Bi_2O_3 concentration, where the peaks are noted in Z_{img} and M_{img} versus frequency spectra in the range of the measured.

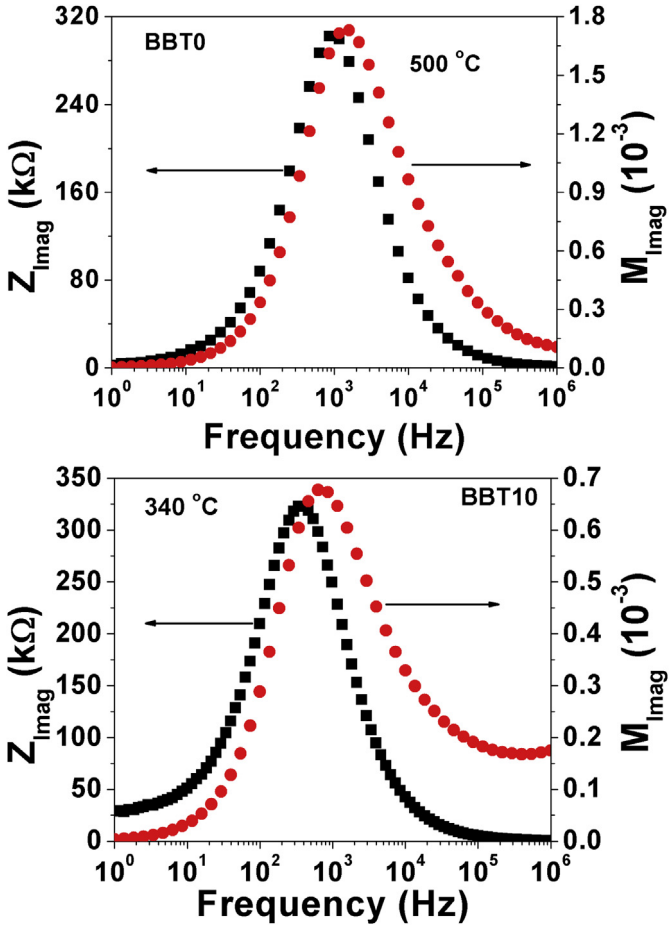

Fig. 7. Variation of Z_{Imag}andM_{Imag} with frequency at the same temperature: a) BBT0 and b) BBT10.

3.5. Nyquist plots

The Fig. 8a-d and its inset shows the Nyquist plot for pure BBT0 and BBT10 for different temperatures over a wide range of frequency (1 Hz–1 MHz). In Fig. 8a and b for BBT0 presents (a) 10 different temperatures (b) fitting spectra data. Fig. 8c and d for BBT10 presents (c) 10 different temperatures (d) fitting spectra data.

The impedance analysis of these material was characterized by the formation of semicircular arcs, whose pattern of evolution changes with increased temperature. The extent of the intercept of the semicircles on the real axis and its number in the spectrum provides information on the kind of electrical processes occurring within the material. The correlation between the arcs and an equivalent electrical circuit is very important to analyze the results, shown in the inset in Fig. 8b and d. The results in Fig. 8 and its inset shows the consistent behavior described. Two R-CPE circuits having different relaxation time constant and connected in series lead to two semicircles, as shown for spectra presented in Fig. 8 for BBT0 and BBT10 samples. As occurring in the case of any other spectroscopy analysis, the separate responses may overlap and the experimental curves must then be resolved into its separated constituent semicircle. Therefore, the equivalent circuit used to fit the spectra consist of a parallel R_1-CPE_1 (constant phase element) connected in series with a parallel R_2-CPE_2. The peak frequency related to grain boundary is smaller than for the grains, due to its large capacity and resistance. The semicircular arc on the highest frequency (R_1-CPE_1) was related to the grain and semicircular arc on the lowest frequency (R_2-CPE_2) was related to the grain boundary.

The CPE component can be connected to the non-ideal behavior of capacitance, with possible origins in a relaxation process with similar relaxation times. The CPE impedance (Z_{CPE}) is given by the following equation:

$$Z_{CPE} = \frac{1}{Q(jw)^{\alpha}} \tag{4}$$

where Q is a proportional factor, w is the angular frequency and α is an empirical exponent with values between 0 and 1. Considering the value of exponent α, CPE has a behavior similar to the component conventionally used in equivalent circuit. The CPE is reduced to resistance and ideal capacitive elements when α is close to zero and 1, respectively. Similar equivalent electric circuit have been used in the literature [26,28–31]. At higher temperatures above 320 °C, the complex impedance plots of BBT generally comprise two overlapping semicircular arcs with its center below the real axis.

The two semicircular features are associated with the dielectric response from the grain, at high frequencies, and the grain boundary, at low frequencies. This can be attributed to the grain boundary because its larger resistance and capacitance, causes the relaxation at lower frequencies compared to the response of the grain.

The origin of semicircular arcs at temperatures above 340 °C(up to 520 °C) suggests that the electrical process in these materials arise basically due to the contributions from grain (bulk) material, and thus can be modeled as an equivalent electrical circuit (inset Fig. 8b and d).

The intercept of each semicircle on the real Z_{Real} axis gives the value of the grain and grain boundary contribution to the resistance. The shape of our data plots suggests that the electrical response is composed of at least two relaxation mechanisms with different relaxation frequencies. Observing an increase in the values of the resistance both grain resistance and capacitance (R_1-

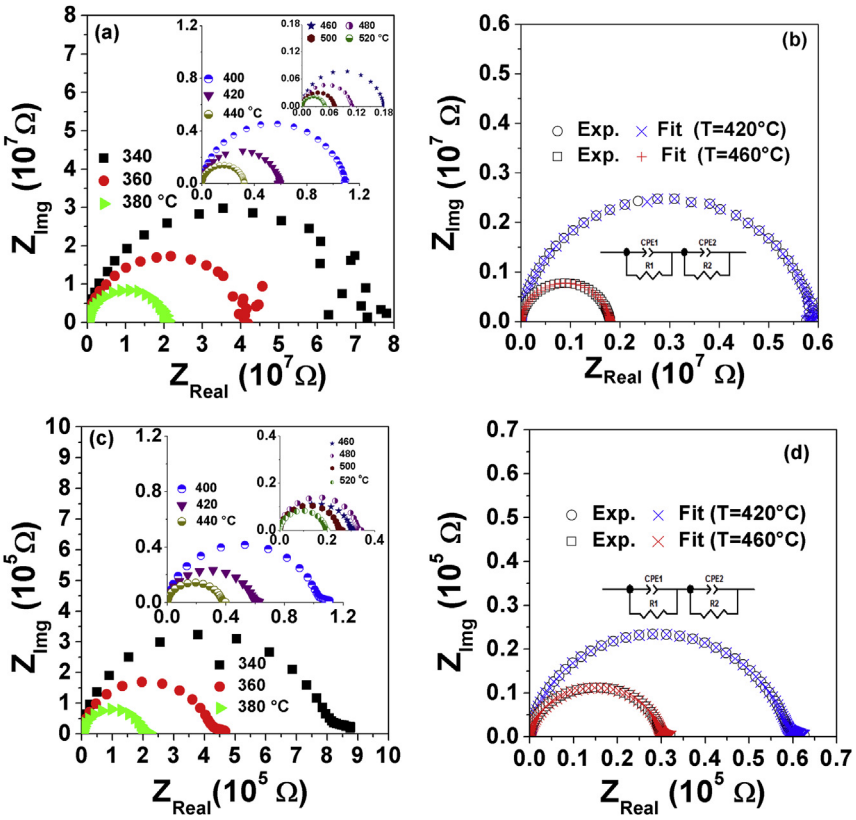

Fig. 8. Nyquist plot and equivalent circuit (with fitting): (a,b) for BBT0 and (c,d) BBT10.

CPE_1) and, grain and capacitance boundary (R_2-CPE_2) values for BBT0, BBT1, BBT2, BBT5 and BBT10 are summarized in Table 1.

It is possible to observe a continuous decreasing in the grain and boundary grain resistance, related herein as R_1 and R_2, respectively. Both grain and boundary grain resistance are found to decrease with increasing temperature values, showing a negative temperature coefficient of resistance (NTCR) behavior [28,32], these results can be explained by the increase of the mobility of charge carriers in the material [28].

Once the time constant (τ) is a parameter that represents the time it takes the system step response to any step input, it is possible to separate its contribution along the electron transport at the grain and grain boundary interface. Fig. 9 exhibits the time constant as a function of temperature for a) grain (τ_1) and b) grain boundary (τ_2) obtained for BBT and BBT10. It is possible to notice in Fig. 9, that both time constants (grain and grain boundary) decrease as a function of increasing temperature, as a result of NTCR and higher mobility of charge carriers. Also, the grain-time constant (τ_1) is up to 55-fold lower than grain boundary-time constant (τ_2).

Moreover, it is a general statement and does not depend on BBT or BBT10 sample materials. Lower values for grain-time constant compared to grain boundary-time constant are related to Debye length in semiconductors,

$$L_D = \sqrt{\frac{\varepsilon k_B T}{q^2 N_d}} \tag{5}$$

where ε is the dielectric permittivity, k_B is the Boltzmann's constant, T is the absolute temperature, q is the elementary charge and N_d is the density of dopants (donor/acceptors). Consequently, in the present case, higher Debye length leads to lower time constant. As the grain boundary presents higher traps density, which acts as carrier recombination, it is expected to lower Debye length at the grain boundary. As a result, higher grain boundary-time constant. Furthermore, it can be also related to the dielectric permittivity, as further discussed. The above discussion, is in agreement with the proposed equivalent electric circuit. Grain boundary process were observed at lower frequency, at Nyquist plot. As stated, $w = t^{-1}$, consequently, higher t values and lower Debye length could be observed at the grain boundary. Finally, among the properties of doped materials e.g. increase carrier concentration, carrier mobility, occupation of interstitial and substitutional sites and segregate to grain boundary can act as parameters to decrease the BBT10-time constant compared to BBT sample materials.

3.6. Dielectric permittivity

Fig. 10a and b shows the temperature dependence of dielectric permittivity (ε_{Real}) of BBT0 and BBT10 compositions at different frequencies (100 Hz-100 kHz). The frequency dispersion of the dielectric permittivity is detected in all samples, here shown for theBBT0 and BBT10 samples. The dielectric permittivity shows a broad diffuse transition around the phase transition temperature (Tm) and a strong frequency dispersion of the dielectric permittivity in all the BBT samples, these results shows an agreement with earlier observations. The frequency dispersion and diffused phase transition of dielectric permittivity at Tm are characteristics associated with ferroelectrics. In the sample BBT0 ceramics, without any excess of Bi_2O_3, a large dielectric dispersion in ε_{Real} below and above Tm is observed with a decrease in ε_{Real} (Tm) with increasing frequency. The frequency dependence of the real part of the dielectric permittivity of the BBT0compositions shows at about Tm~ 450 °C (100 Hz) the maximum value of the dielectric

Table 1
Electrical parameters values obtained from impedance spectra fitting for BBT and doped contents.

Sample	T (°C)	CPE1-T	CPE1-P	R1	CPE2-T	CPE2-P	R2
BBT0	340 °C	4,94E-10	0,96586	8,8423E6	3,897E-10	0,96982	6,1395E7
	380 °C	6,07E-10	0,97105	3,5465E6	5,835E-10	0,96345	1,6782E7
	420 °C	7,245E-10	0,97802	538820	5,157E-10	0,96603	5,2735E6
	460 °C	8,049E-10	0,98542	177270	4,849E-10	0,96788	1,6111E6
	500 °C	5,503E-10	0,98984	85295	4,351E-10	0,96025	627030
	520 °C	4,244E-10	0,99168	75474	4,234E-10	0,95637	426630
BBT1	340 °C	4,788E-10	0,96886	1,5092E7	6,533E-10	0,95946	5,6231E7
	380 °C	7,682E-10	0,97058	3,3078E6	7,206E-10	0,96054	1,6581E7
	420 °C	1,020E-9	0,97535	745080	7,019E-10	0,96907	4,7942E6
	460 °C	1,121E-9	0,98474	138270	5,848E-10	0,96972	1,5526E6
	500 °C	8,031E-10	0,98984	52386	5,263E-10	0,96032	542290
	520 °C	5,683E-10	0,99254	51397	5,021E-10	0,95835	355750
BBT2	340 °C	4,701E-10	0,96389	1,6541E7	5,358E-10	0,96789	6,7913E7
	380 °C	7,340E-10	0,97434	3,2867E6	6,207E-10	0,96334	1,7753E7
	420 °C	9,325E-10	0,97978	770000	6,052E-10	0,97141	5,1725E6
	460 °C	1,063E-9	0,98829	141400	4,842E-10	0,97343	1,691E6
	500 °C	7,475E-10	0,99283	58773	4,181E-10	0,96584	648080
	520 °C	4,969E-10	0,99461	66238	4,151E-10	0,96217	436490
BBT5	340 °C	4,769E-10	0,96845	1,1528E7	1,1528E7	0,95867	3,9899E7
	380 °C	7,116E-10	0,97248	1,1528E7	8,611E-10	0,95921	9,838E6
	420 °C	9,948E-10	0,98045	496000	7,233E-10	0,96844	3,0285E6
	460 °C	9,867E-10	0,989	105700	5,815E-10	0,97013	988010
	500 °C	5,377E-10	0,9938	73235	5,792E-10	0,95963	366620
	520 °C	3,702E-10	0,99354	76810	6,024E-10	0,95611	237890
BBT10	340 °C	9,543E-10	0,9524	303710	2,589E-9	0,91984	530990
	380 °C	1,578E-9	0,94797	83870	5,341E-9	0,90577	125620
	420 °C	1,899E-9	0,95789	538820	6,157E-9	0,90838	37929
	460 °C	1,517E-9	0,97748	8201	6,088E-9	0,8945	22480
	500 °C	9,730E-10	0,98255	5929	2,119E-9	0,92729	19395
	520 °C	7,713E-10	0,98543	4630	1,983E-9	0,92087	15084

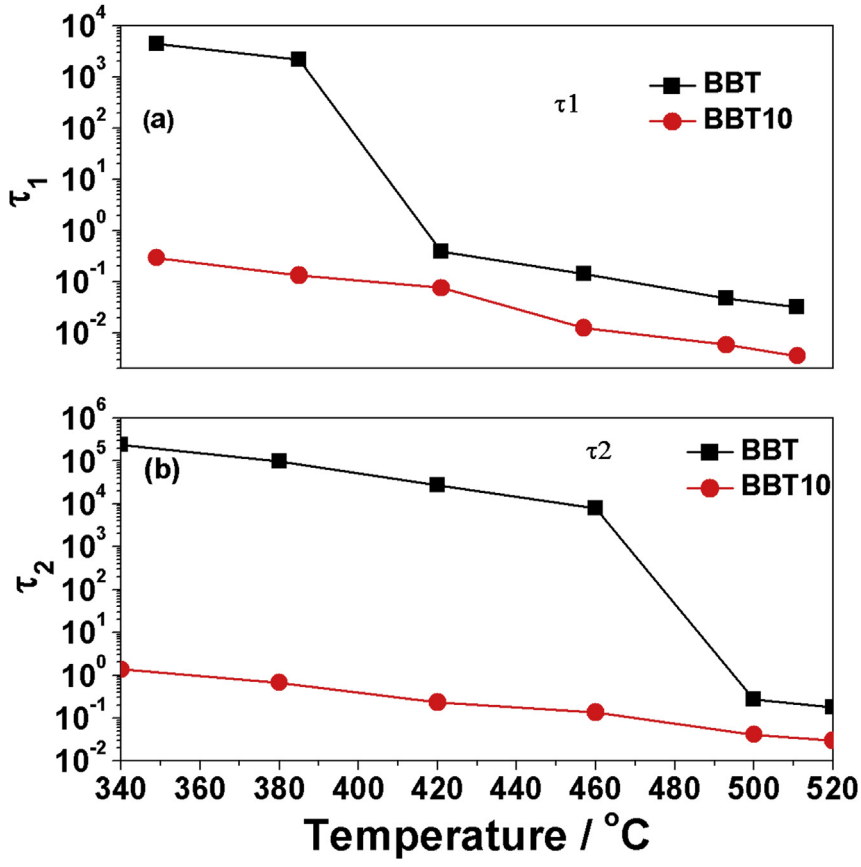

Fig. 9. Time constant related to a) grain and b) grains boundary as function of temperature for BBT and BBT10 doped sample materials.

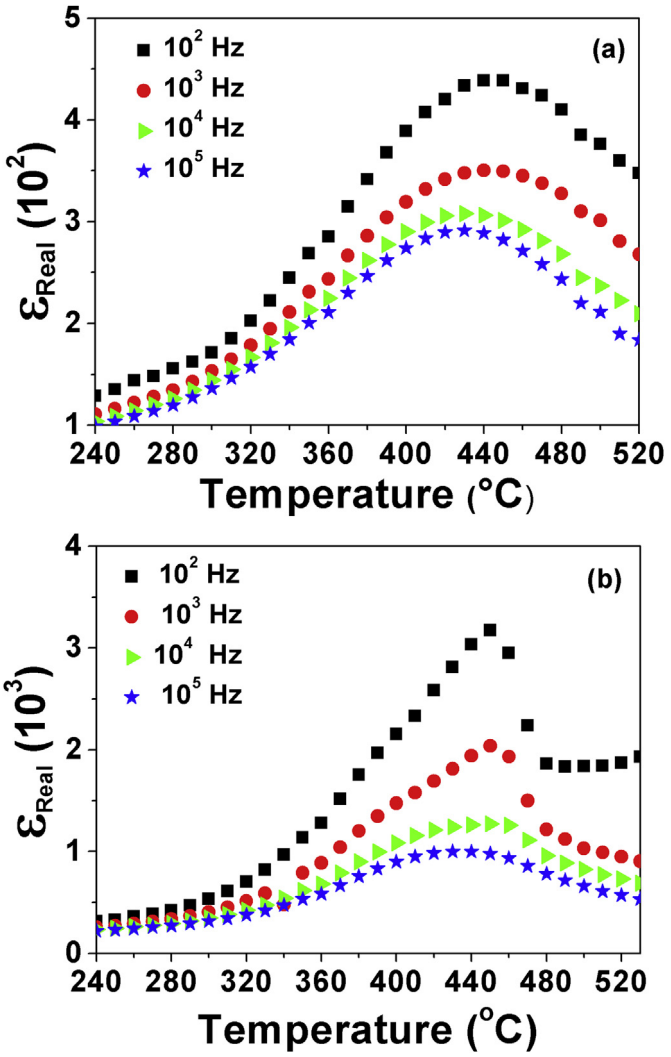

Fig. 10. Temperature and frequency dependence of dielectric permittivity (ε_{Real}) of BBT ceramic$_s$ with: a) BBT0 and b) BBT10.

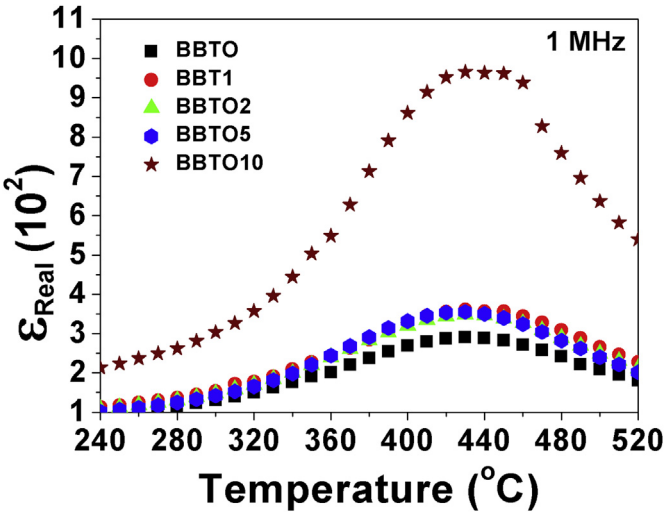

Fig. 11. Temperature dependent dielectric behavior of BBT ceramics measured at 1 MHz frequency.

permittivity decreases with an increase in frequency and the real part of the dielectric permittivity shows a diffuse transition maximum.

In this study,no change in Tm was observed in the sample BBT10 (Fig. 10b) at different frequencies. Moreover, all the BBT compositions prepared, varying amount of excess Bi_2O_3 exhibited an increase in the maximum dielectric permittivity at *Tm*.

Fig. 11 shows the temperature dependence of the dielectric permittivity (ε_{Real}) of the BBTceramic at different concentrations of Bi_2O_3 measured at 1 MHz. In earlier reports an excess of bismuth has been shown to decrease the ferroelectric phase transition temperature *Tm*. The value of the dielectric permittivity at a temperature of 240 °C was observed to be ~100 for BBT0 ceramic, but with an increase in the concentration of Bi_2O_3 this value increased. It is important to note that the temperature dependence of the dielectric permittivity shown in Figs. 10 and 11 clearly indicates the presence of a structural phase transition that has been observed near 450 °C.

3.7. Conductivity

Fig. 12a-b shows the variation of the conductivity (σ_{Real}) as a function of frequency in temperatures (340–520 °C). According to the results presented, both conductivity plots show a frequency dispersion at lower frequency regions that shifts to higher frequencies regions with an increase in temperature, implying a Jonscher-type universal power law ($\sigma_{ac} = \sigma_{dc} + A\omega^n$), where σ_{dc} is conductivity at a particular temperature in the frequency of 1 Hz, A is the temperature dependent constant and *n* is the temperature dependent exponent over range of $0 \leq n \leq 1$. The parameter *A* determines the strength of the polarizability and represents the degree of interaction between mobile ions and the lattices around them. Following the concepts of Jonscher [33], relaxation phenomena arising due to mobile charge carriers is associated with the origin of the frequency-dependence of the conductivity lies. Due a mobile charge carrier hops to a new site from its original site; it remains confined in a state of displacement between two potential energy minima. Low frequency region we consider the DC conductivity, this value increases with an increase in temperature. With this value,one estimates the activation energy of the charge carriers. In the high frequency region, all curves tend to merge to the same value. The conductivity study on the dielectric specimen at different temperatures gives information on the dominant conducting species within the sample. Fig. 12a shows data on BBT0 and Fig. 12b to BBT10. It is observed that for the sample with 10-wt% Bi_2O_3, the conductivity value significantly increases, by almost two orders of magnitude.

Analyzing the graphs of the DC conductivity (Fig. 12a and b) the charge carrier mechanism can be interpreted as a process of jumping between two sites separated by an energy barrier, this results follows the Arrhenius law $\left(\sigma = \sigma_0 exp^{-\left(\frac{E_a}{kT}\right)}\right)$ for all temperatures. Where σ_o is the pre-exponential factor, E_a the activation energy, k = Boltzmann constant and T is temperature in Kelvins. According to Khokhar et al. [34] in the low frequency region the *dc* conductivity (at high temperature), there is a diffusion of charge carriers, which is related with a ferroelectric phase transition. In addition, there are space charge contributions long-range charges. Kumar et all [26] states that the conduction occurs through hopping of charges particles from one localized state to another resulting in the long-range translational motion of charge carriers, the movement of charged particles contributes to the DC conductivity.

From the results presented in the Fig. 12b the conductivity at all temperatures along with the results presented in Fig. 6b (for frequency peak maximum) are shown in Fig. 13 for sample BBT10. The

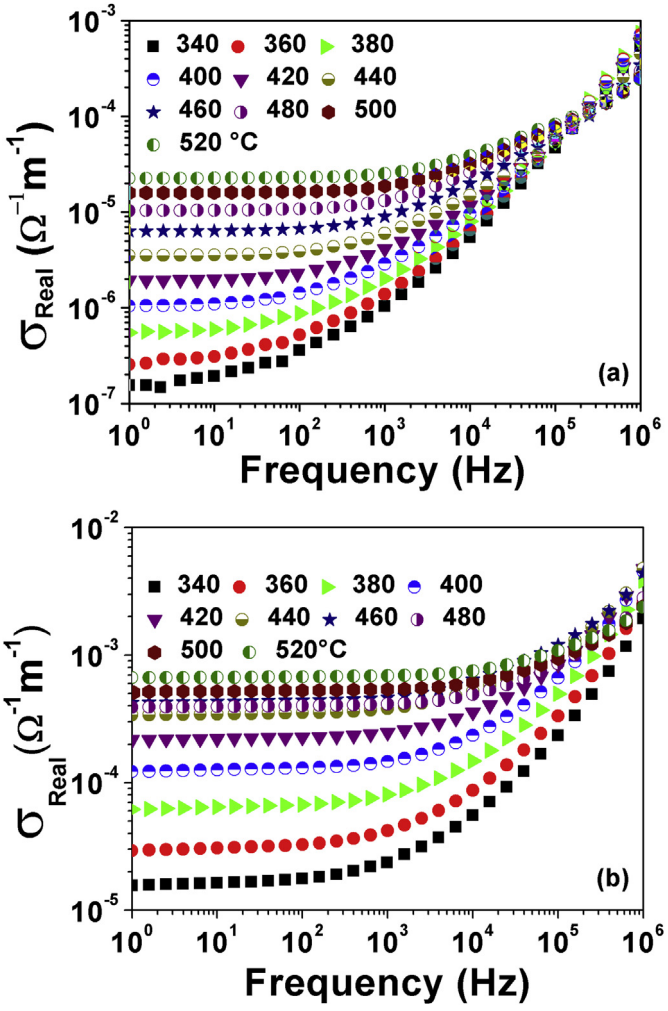

Fig. 12. Variation of conductivity as a function of frequency at different temperature for: a) BBT and b) BBT10.

variation of σ_{dc} (1 Hz) vs. 10^3/T and f_{peak} (peak maximum, Fig. 6b vs. 10^3/T with temperature follows the Arrhenius relation

$$\left(\sigma_{dc} = \sigma_0 exp^{-\left(\frac{E_a}{kT}\right)}\right) \quad \text{or} \quad \left(f_{peak} = f_0 exp^{-\left(\frac{E_a}{kT}\right)}\right).$$

In Fig. 13 for each value of σ_{dc} and f_{peak}, the occurrence of different slopes over the different temperature regions can be connected to the presence of multiple conduction processes in these samples with different activation energies. The estimated activation energy (E_a) of the sample over the range of 340–440 °C is 1.21 eV (from σ_{dc} versus 1/T K) and 0.94 eV (from f_{peak} versus 1/T k) and over the range 490–530 °C the value for *Ea* is 0.81 eV (fromσ_{dc} versus 1/T K)and 1.21eV (from f_{peak} versus 1/T(K)). The different values of the activation energy from modulus and conductivity spectra is a strong indication that the relaxation and conductivity processes are presents.

These results can be explained because the complex electric modulus is important in the analysis of the bulk properties,as apparent conductivity relaxation times is present in the material. This means that the charge carriers are responsible for the conduction and relaxation processes at lower temperatures. Above the transition temperature, the largest contribution to this energy is

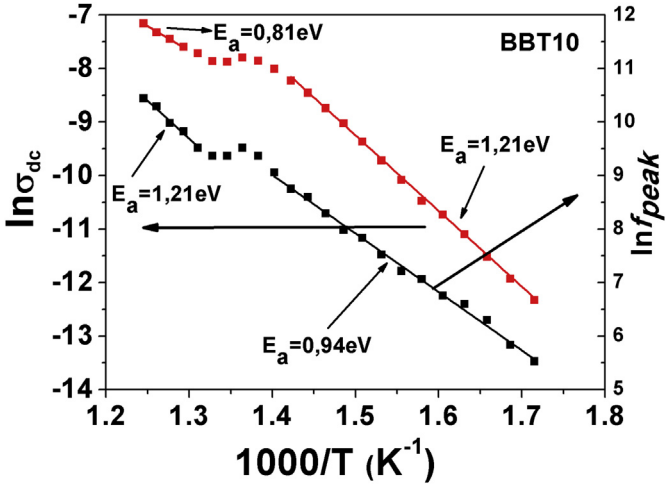

Fig. 13. Variation of dc conductivity and f_{peak} with inverse of absolute temperature for BBT10.

associated with the bulk of the material (modulus spectra). Table 2 shows the values of the activation energies obtained from the peak frequency (M_{Img}) and from the conductivity (dc) at 1 Hz in all samples.

4. Scanning electronic microscopy

Fig. 14a and b show the fractured unpolished FE-SEM of the samples BBT0 and BBT10. It's possible observe that with increase amount of Bi_2O_3 in the structure of $BaBi_4Ti_4O_{15}$ occurs an increase in the density of the samples. This increase of density at function with $Bi_2O_3$was attributed at formation of a liquid phase of the Bi_2O_3 and contributed at mass transfer in the process of sinterization [15]. Moreover, the addiction in excess of Bi_2O_3 contributed to decrease of oxygen vacancies in the structure of $BaBi_4Ti_4O_{15}$ formed in the sintering process, thus, improving the dielectric permittivity, conductivity and impedance response [35,36].

5. Conclusion

The results shown here report studies structural properties, impedance spectroscopy and electrical modulus properties of BBT ceramics modified with 0, 1, 2, 5 and 10% of Bi_2O_3, synthesized via the solid-state reaction route.

The Rietveld refinement confirmed the formation of a tetragonal structure with a non-polar space group 14/mmm for BBT calcined at a temperature of850 °C for 3hs with increasing in the fundamental crystallographic parameter *c*/*a* of 10.8074 up to 10.8900 for BBT compared to BBT-doped materials. The impedance spectroscopy plots show that the material exhibits an electrical transport process (conduction) due the grain (bulk) and grain boundary (interface), and a temperature-dependent relaxation phenomenon. With the impedance spectroscopy it is possible to separate the grain and grain boundary contributions in the material. Both resistances decrease with a rise in temperature for all the compositions. The complex modulus reveals that this material exhibits a diffuse type ferroelectric phase transition with a transition temperature well above the room temperature (Tm ~ 450 °C).

The sample exhibits a dielectric relaxation to be of a non-Debye type and the relaxation frequency move to higher frequencies with an increase in temperature. The frequency dependence of the imaginary part of the impedance and the imaginary part of the modulus suggests the presence of short-range motion of charge

Table 2
Activation energies values obtained from f_{peak} and σ_{dc} impedance spectra for BBT and doped contents.

	BBT0		BBT1		BBT2		BBT5		BBT10	
	Ea < Tm, Ea > Tm		Ea < Tm, Ea > Tm		Ea < Tm, Ea > Tm		Ea < Tm, Ea > Tm		Ea < Tm/Ea > Tm	
Activation energy f_{pico}	1.39	1.46	0.35	0.43	0.55	1.58	0.69	1.41	0.94	1.21
Activation energy σ_{dc}	0.78	1.20	1.52	1.27	0.77	1.06	0.92	1.15	1.21	0.81

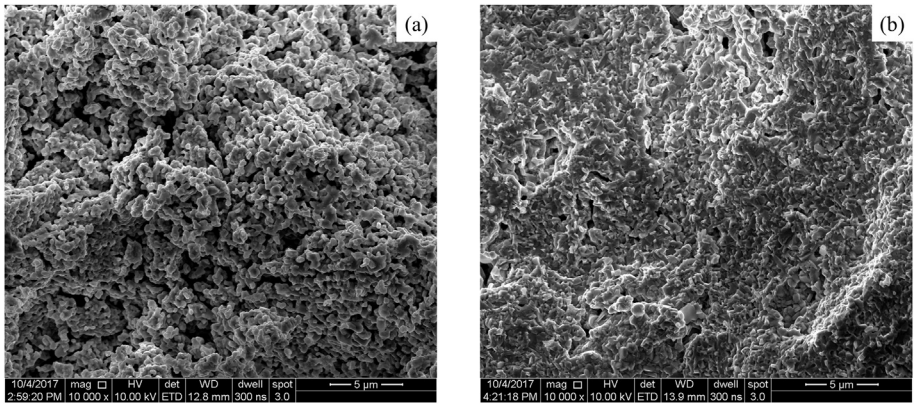

Fig. 14. FE-SEM images of the unpolished fractured pellets for a) BBT and b) BBT10.

carries. The value of conductivity increases with temperature the increase in the value of the conductivity is due to thermal activation of the conducting species in the material, but the conductivity decreases as the Bi_2O_3 content increases. The increase in the conductivity value at increased temperature indicates the onset of semiconductor behavior of the material. The relaxation frequency computed from the M_{Img} peak maxima and the DCconductivity from conductivity data at lower temperatures followed Arrhenius-type behavior with different slopes in the temperature range, the turning point occurs in Tm.

Acknowledgements

This work was partly sponsored by CNPq (427161/2016-9), CAPES and FAPEMAT (214599/2015) Brazilian funding agencies. The authors acknowledge with thanks the contributions of Prof. Dr. David P. Cann for English revision.

References

[1] H. Ogawa, M. Kimura, A. Ando, Y. Sakabe, Temperature dependence of piezoelectric properties of grain-oriented $CaBi_4Ti_4O_{15}$ ceramics, Jpn. J. Appl. Phys. 40 (2001) 5715–5718.
[2] A. Chakrabarti, J. Bera, T.P. Sinha, Dielectric properties of $BaBi_4Ti_4O_{15}$ ceramics produced by cost-effective chemical method, Phys. B Cond. Matter 404 (8–11) (2009) 1498–1502.
[3] A.Q. Jiang, Z.X. Hu, L.D. Zhang, The induced phase transformation and oxygen vacancy velaxation in La-Modified bismuth titanate ceramics, Appl. Phys.Lett 74 (1) (1999) 114–116.
[4] R.E. Newnham, R.W. Wolfe, J.F. Dorrian, Structural basis of ferroelectricity in the bismuth Titanate Family, Mater. Res. Bull. 6 (1971) 1029–1040.
[5] B. Aurivillius, "Mixed Bismuth Oxides with Layer Lattices, III Structure of $BaBi_4Ti_4$ O_{15},"Ark.Kemi1 519–527(950).
[6] C.-H. Lu, C.-Y. Wen, New non-fatigue ferroelectric thin films of barium bismuth tantalite, Mater. Lett. 38 (278–282) (1999).
[7] H. Du, Y. Li, H. Li, X. Shi, C. Liu, Relaxor behavior of bismuth layer-structured ferroelectric ceramic with m=2, Solid State Commun. 148 (2008) 357–360.
[8] R.Z. Hou, X.M. Chen, Y.W. Zeng, Diffuse ferroelectric phase transition and relaxor behaviors in Ba-based bismuth layer-structured compounds and La-substituted $SrBi_4Ti_4O_{15}$, J. Am. Ceram. Soc. 89 (2006) 2839–2844.
[9] J.R. Macdonald, Impedance Spectroscopy: Emphasizing Solid State Materials and Systems, Wiley, New York, 1987 (Chapters 2 and 4).
[10] A.R. West, D. Sinclair, N. Hirose, Characterization of electrical materials, especialy ferroelectrics, by impedance spectroscopy, J. Electroceram 1 (1) (1997) 65–71.
[11] S. Kumar, K.B.R. Varma, Relaxor Behaviour in $BaBi_4Ti_4O_{15}$ ceramics fabricated using the powders obtained by mechanochemically assisted synthesis route, Bull. Mater. Sci. 37 (6) (2014) 1233–1241.
[12] B. Tanmaya, H.R. Kumar, N.S. Sekhar, M. Avinna, A. Sahid, Frequency and temperature dependence behaviour of impedance, modulus and conductivity of $BaBi_4Ti_4O_{15}$ Aurivillius Ceramic, Process. Appl. Ceram. 8 (3) (2014) 145–153.
[13] X.G. Tang, K.-H. Chew, H.L.W. Chan, Diffuse phase transition and dielectric tunability of $Ba(Zr_yTi_{1-y})O_3$ relaxor ferroelectric ceramics, ActaMaterialia 52 (2004) 5177–5183.
[14] A. Chakrabarti, J. Bera, T.P. Sinha, Dielectric properties of $BaBi_4Ti_4O_{15}$ ceramics produced by cost-effective chemical method, Phys. B 404 (2009) 1498–1502.
[15] A. Khokhar, P.K. Goyal, O.P. Thakur, K. Sreenivas, Effect of excess of bismuth doping on dielectric and ferroelectric properties of $BaBi_4Ti_4O_{15}$, Ceram. Int. 41 (2015) 4189–4198.
[16] A.C. Larson, R.B.V. Dreele, General Structure Analysis System (GSAS), Los. Alamos National Laboratory Report LAUR 86-748, 2004.
[17] B.H. Toby, EXPGUI, a graphical user interface for GSAS, J. Appl. Cryst. 34 (2001) 210–213.
[18] P. Thompson, D.E. Cox, J.B. Hasting, Rietveld refinement of debye–scherrer synchrotron x-ray data from Al_2O_3, J. Appl. Cryst. 20 (1987) 79–83.
[19] P.W. Stephens, Phenomenological model of anisotropic peak broadening in powder diffraction, J. Appl. Cryst. 32 (1999) 281–289.
[20] N.H. March, Electron Density Theory of Atoms and Molecules, Academic Press, New York, 1992. Chap. 1.
[21] J. Tellier, Ph. Boullay, M. Manier, D. Mercurio, A comparative study of the aurivillius phase ferroelectrics $CaBi_4Ti_4O_{15}$ and $BaBi_4Ti_4O_{15}$, J. Solid State Chem. 177 (2004) 1829–1837.
[22] B.J. Kennedy, Y. Kubota, B.A. Hunter, Ismunandar, K. Kato, Structural phase transitions in the layered bismuth oxide $BaBi_4Ti_4O_{15}$, Solid State Commun. 126 (2003) 653–658.
[23] P.L. Bernardo, L. Ghivelder, G.G. Eslava, H.S. Amorim, I. Felner, et al., Monoclinic distortion and magnetic coupling in the double perovskite $Sr_{2-}xCaxYRuO_6$, J. Solid State Chem. 220 (2014) 270–276.
[24] J.D. Bobic, M.M.V. Petrovic, J. Banys, B.D. Stojanovic, Electrical properties of niobium doped barium bismuth-titanate ceramics, Mater. Res. Bull. 47 (2012) 1874–1880.
[25] A.C. Tomkiewicz, M. Tamimi, A. Huq, S. McIntosh, Oxygen transport pathways in ruddlesden-popper structured oxides revealed via in situ neutron diffraction, J. Mater. Chem. A 43 (3) (2015) 21864–21874.

[26] S. Kumar, K.B.R. Varma, Dielectric relaxation in bismuth layer-structured $BaBi_4Ti_4O_{15}$ ferroelectric ceramics, Curr.Appl. Phys. 11 (2011) 203–210.
[27] D.C. Sinclair, A.R. West, Impedance and modulus spectroscopy of semiconducting BaTiO3 showing positive temperature coefficient of resistance, J. Appl. Phys. 66 (8) (1989) 3850–3856.
[28] A. Benali, M. Bejar, E. Dhahri, M.F.P. Graca, L.C. Costa, Electrical conductivity and ac dielectric properties of $La_{0.8}Ca_{0.2}$-xPbxFeO$_3$ (x = 0.05, 0.10 and 0.15) perovskite compounds, J. Alloys Comp 653 (2015) 506–512.
[29] F. Meng, T. Xia, J. Wang, Z. Shi, H. Zhao, Praseodymium-deficiency $Pr_{0.94}BaCo_2O_6$-δ double perovskite: a promising high performance cathode material for intermediate-temperature solid oxide fuel cells, J. Power Sources 293 (2015) 741–750.
[30] L. Gan, Q. Zhong, X. Zhao, Y. Song, Y. Bu, J. Alloys Comp 655 (2016) 99–105.
[31] H. Khelifi, I. Zouari, A. Al-Hajry, N. Abdelmoula, D. Mezzane, et al., Ac conductivity and ferroelectric phase transition of $Bi_{0.7}(Ba_{0.8}Sr_{0.2})_{0.3}Fe_{0.7}Ti_{0.3}O_3$ ceramic, Ceram. Int. 41 (2015) 12958–12966.
[32] J.C. Debnath, A.M. Strydom, Large low field magneto-resistance and temperature coefficient of resistance in $La_{0.8}Ca_{0.2}MnO_3$ epitaxial thin film, J. Alloys Comp 621 (2015) 7–11.
[33] A.K. Jonscher, The 'universal' dielectric response, Nature 267 (1977) 673–679.
[34] A. Khokhar, M.L.V. Mahesh, A.R. James, P.K. Goyal, K. Sreenivas, Sintering characteristics and electrical properties of $BaBi_4Ti_4O_{15}$ ferroelectric ceramics, J. Alloys Comp 581 (2013) 150–159.
[35] S. Kumar, K.B.R. Varma, Influence of lanthanum doping on the dielectric, ferroelectric and relaxor behavior of barium bismuth titanate ceramics, J. Phys. D. Appl. Phys. 42 (075405) (2009).
[36] J.D. Bobic, M.M. Vijatovic, S. Greicius, J. Banys, B.D. Stojanovic, Dielectric and relaxor behavior of $BaBi_4Ti_4O_{15}$, J. Alloys Comp. 499 (2010) 221–226.
[37] D. Peng, H. Zou, C. Xu, X. Wang, X. Yao, Er doped $BaBi_4Ti_4O_{15}$ multifunctional ferroelectrics: Up-conversion photoluminescence, dielectric and ferroelectric properties, J. Alloys Comp. 552 (2013) 463–468.